Synchronization of Oscillations and Propagation of Excitations in Circular and Linear Arrays of Coupled CSTRs

V. Nevoral, V. Votrubová, P. Hasal,* L. Schreiberová, and M. Marek

Department of Chemical Engineering and Center for Nonlinear Dynamics of Chemical and Biological Systems, Faculty of Chemical Engineering, Institute of Chemical Technology, Prague, 166 28 Prague 6, Czech Republic

Received: February 24, 1997; In Final Form: April 25, 1997[⊗]

Synchronizations of oscillatory regimes of the Belousov−Zhabotinskii (BZ) reaction in a circular array of three identical CSTRs coupled via symmetric passive diffusion/convection mass transfer were studied experimentally. Stability of symmetric and asymmetric phase-shifted oscillatory regimes with respect to variations of the coupling strength among the reaction cells was examined. The all-in-phase regime was found to be the only regime stable over the entire range of coupling strength values. Phase-shifted oscillatory regimes were found to be stable only within a narrow interval of very low coupling strength values. Spontaneous transitions of the phase-shifted regimes to the synchronized mode due to stochastic fluctuations of the coupling strength were observed. Numerical simulations with the four-variable Oregonator based model of the BZ reaction qualitatively confirmed the experimental findings. Propagation of an excitable response to periodic pulsed stimulations in a linear three-array of coupled chemical excitators (Belousov−Zhabotinskii reaction) was studied in dependence on the coupling strength, on the excitability level of the reaction mixture, and on the period and amplitude of pulse stimulation. Regimes of complete and partial propagation of the excitable response and the regimes of partial and complete propagation failure were observed. Numerical simulations predict qualitatively well excitatory regimes observed in experiments.

1. Introduction

Chemical oscillators and excitators are encountered both as low-dimensional, lumped parameter systems, *e.g.*, continuous stirred tank reactors (CSTRs), described by a set of nonlinear ordinary differential equations, and as infinite-dimensional distributed parameter systems, *e.g.*, excitable reaction−diffusion systems, usually described by a set of partial differential equations. Motivation for the study of networks of coupled chemical oscillators and excitators stems both from their significance to an interpretation and understanding of observed spatiotemporal patterns in chemical systems and from their importance for the interpretation of the mechanism of generation of spatiotemporal patterns in much more complex biological systems. Synchronization among nonlinear oscillators often plays a crucial role in living organisms; for example, various biorhythms (myocardial cells, neural cells, and metabolic activities) exhibit synchronization. The evaluation of received information occurs by synchronized firings of groups of individual units both at the level of receptors (*e.g.*, evaluation of visual information in the retina) and at the level of neurons in the cortex. The mechanism of response of groups of coupled cells to stimulations, synchronization of evoked firings in cells, and resulting spatiotemporal patterns in the groups of cells are therefore a subject of continuous interest. Circularly coupled nonlinear oscillators, including three-membered rings, are specifically used to model mammalian intestinal activity, and various cyclic symmetrically coupled nonlinear oscillators are used to describe the neurophysiological mechanisms underlying the control of insect locomotion.[1,2] Phase relations among individual oscillations serve for coding of various locomotion patterns.[1] The region of stability and robustness to noise of individual phase-locked regimes of oscillators is of particular interest, *cf. e.g.*, Collins and Stewart.[2]

Signal and information processing in cascades of units (*e.g.*, cell receptors, neurons, and excitable cells) takes the form of a combination of firings ("digital" signals) with spreading spatiotemporal patterns of specific chemical species (*e.g.*, Ca^{2+} ions[4]). Temporal and spatial characteristics of sequences of firings in individual units seem to be used for the encoding of information, for example in neural systems,[3,4] where timing of an event in the exterior of the cells, the timing of the representation of that event within the cell, and relative timing of spikes between two or more cells are main aspects of this process. Detailed studies of quantitative relations of spatiotemporal firing patterns in cascades of excitable chemical units can serve the purpose of testing the available patterns in coupled excitable cell systems.

Signal and information processing also can take place in systems of coupled bistable units. Arrays of such units may serve, for example, for pattern recognition, as documented recently by experiments of Laplante *et al.*,[6] who performed experiments with the bistable iodate−arsenous acid reaction in an eight-array of mass-flow coupled CSTRs. Using a Hebbian type rule for setting the coupling strengths (intensity of reciprocal pumping by peristaltic pumps) between all pairs of CSTRs, the authors trained the array to recall stored patterns from similar input patterns.

Experiments with model chemical systems can usually be performed under well-controlled experimental conditions and interpreted on the basis of well-founded and documented kinetic models. Recently Yoshikava *et al.*[5] studied synchronization of Briggs−Rauscher reaction oscillators in the cyclic system of three batch stirred reactors coupled via mass exchange through small openings in reactor bottoms and in the system of three water−salt oscillators immersed in a common bath. It has been found in both systems that the oscillations stabilize spontane-

* Author to whom correspondence should be addressed. e-mail: hasalp@tiger.vscht.cz.

[⊗] Abstract published in *Advance ACS Abstracts,* June 1, 1997.

S1089-5639(97)00672-5 CCC: $14.00

ously in a triphasic mode (phase shifts 120°). Among the chemical oscillators, coupling between two or more continuous flow stirred tank reactors with Belousov−Zhabotinsky (BZ) reaction or other reactions was a subject of extensive theoretical and experimental studies.[7−29] Three different ways of coupling were used: (i) direct mutual mass-flow coupling[7−19] (ii) coupling by pumping,[20−25] and **(**iii) electric current or potential coupling.[26−29]

Marek and Stuchl[7] studied synchronization of oscillations in two interacting CSTRs with the BZ reaction. A passive symmetric mass transfer coupling of the CSTRs was used. Different frequencies of oscillations in both reaction cells were set by means of different reaction temperatures. Phenomena such as synchronization at a common frequency, synchronization at subharmonics of a common frequency, rhythm splitting, and amplitude amplification were observed, depending on the coupling strength and the ratio of autonomous frequencies of both oscillators. Yoshimoto *et al.*[20] studied experimentally synchronization phenomena in a circular three-array of CSTRs coupled via pumping by peristaltic pumps. Both symmetric and asymmetric coupling was studied; the asymmetry of the coupling was set up by adjustments of the CSTRs volumes. A wide variety of dynamic modes were observed: a quasiperiodic state, a biperiodic mode, synchronized modes, and an "all-death" mode (no oscillations in either CSTR). Large differences in the structure and stability of detected dynamic modes were observed when comparing symmetric and asymmetric coupling. Doumbouya *et al.*[17] studied the oscillatory BZ reaction in two CSTRs serially coupled via direct mutual mass-flow coupling. They observed a sequence of periodic, quasiperiodic, and chaotic states with decreasing flow rate through the system. The effects of varying coupling strength and volume ratio of both reaction cells were also studied. The variation of the volume ratio altered strongly the transition to chaotic oscillations. The partially reversible Oregonator model was adopted for numerical simulations, and the results of simulations agreed qualitatively with experimental observations. Hauser and Schneider[18] studied interactions of chaotic regimes of the BZ reaction in two CSTRs coupled via direct mutual mass-flow coupling. A synchronization of both chaotic states was observed at higher coupling strengths. The mutual correlation of chaotic states decreased with the decreasing coupling intensity. Schneider *et al.*[28] and Zeyer *et al.*[29] investigated dynamics of electrochemical potentials generated in two CSTRs with the BZ reaction in the oscillatory regime coupled both via direct mutual mass-flow coupling and passive electrical connection (Pt electrodes connected through external resistance). They detected a rich variety of periodic, quasiperiodic, and chaotic alternating potential signals depending on the strength of the electrical coupling. Zeyer *et al.*[19] also studied dynamical modes of the BZ reaction in two direct mass-flow coupled CSTRs, where the coupling strength (the flow rate between the reactors) was proportionally controlled according to the difference of (time-delayed) actual and time-averaged concentration of Ce^{4+} ions.

Excitable lumped parameter chemical reaction systems can be used as well-defined models of nonlinear behavior of continuous excitable media that prevail in biology. The experimental results from chemical systems are more easy to interpret, and the generic and robust results can be helpful in the analysis of more complex biological excitable systems. Dynamic structures observed in nonlinear and nonequilibrium excitatory externally periodically driven systems share a number of common features, as demonstrated recently in the studies of forced excitable chemical systems.[30−36]

Marek and Schreiber[30] summarized dynamical regimes encountered in periodically forced coupled chemical oscillators and excitators (with special emphasis on appearance of chaotic behavior). They analyzed a hierarchical structure of arising resonance and excitation diagrams and on several selected examples demonstrated approaches and techniques used for the analysis of such systems. Nonlinear resonance regimes arising as a response of excitable chemical medium in a CSTR to single or periodic stimulations by concentration pulses were also studied experimentally.[31,32] One-dimensional maps called phase excitation curves (PECs) have been introduced for the description of observed resonances. The conditions necessary for the validity of predictions obtained on the basis of such maps have been verified by application to several kinetic models.[33,34] The use of PECs for the prediction of dynamics of periodically perturbed BZ reaction was studied by Dolník and Marek.[33] Dolník *et al.*[34] studied numerically responses to single and periodic pulse perturbations in two model excitable systems: the four-variable extended Oregonator model of the BZ reaction and the six-variable model of the chlorite−iodide reaction. The PECs obtained from the analysis of the response of an excitable system to single perturbations at various phases of the excitation cycle enabled precise prediction of the behavior of the system affected by periodic perturbations. The analysis of spatiotemporal patterns of excitations in arrays of coupled reaction cells with time delay was the subject of another study.[37] Single firing and finite sequences of firings were observed for both reaction systems, while permanent sequences of firings were detected only in the BZ system. The excitable response of two CSTRs with the BZ reaction coupled via direct mutual mass-flow coupling to both single pulse and periodically repeated perturbations by small additions of Ag^+ ions was studied by Kosek *et al.*[35,36] The excitation diagrams with the dependence of the particular dynamic modes on the period and the amplitude of perturbations were constructed on the basis of both experimental data and numerical simulations. Periodic and aperiodic regimes (both synchronized and unsynchronized) were observed together with the propagation failure phenomenon, *i.e.* no propagation of the excitable response from the first (stimulated) reactor to the unperturbed one in a certain range of amplitudes of the stimulation and intensity of the mass coupling. Even though there exists a large body of mostly theoretical literature on the modeling of biological forced excitable systems such as neuronal cells, pancreatic β-cells, and cardiac cells, *cf., e.g.,* Alexander *et al.*,[38] Othmer,[39] and Holden *et al.*,[40] there have until now been no direct detailed comparisons of the structure of the phase-locked excitable regimes (excitation propagation regimes) in more than two coupled cells with the results of the study of a proper mathematical model. This is one of the purposes of this paper.

In this paper we shall first present results of an experimental study of synchronization phenomena in a circular three-array of CSTRs with the BZ reaction where all reactors are in the oscillatory regime and are coupled via symmetric direct mutual mass-flow coupling. The estimates of regions of stability of individual phase-locked regimes and the effects of noise in the coupling will be established. Then the results of experiments on the propagation of excitable response to periodic pulsed stimulation in the linear three-array of coupled CSTRs with the BZ reaction in the excitable regime are described. The results of experiments are compared to results of numerical simulations.

2. Experimental Section

2.1. Reactors. All experiments were carried out in an experimental setup similar to that used in experiments with two cells by Kosek and Marek.[35] The system of three CSTRs (reaction cells) with direct mutual mass flow coupling, schematically depicted in Figure 1, was used instead of the two-

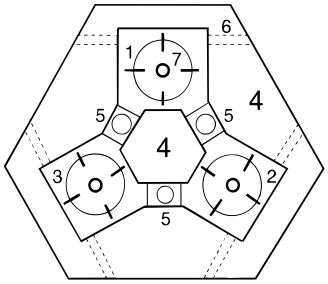

Figure 1. Top view of the reaction cell system: 1, 2, 3, reaction cells; 4, acrylic glass block; 5, connecting openings with movable barriers; 6, holes with quartz-glass windows for the light beam; 7, stirrers. The cells are covered by a common Teflon lid with openings for electrodes, stirrer shafts, thermistors, and inlet and outlet of reaction liquid.

cell system. Each cell (volume $V = 30$ cm^3) is a cube-shaped cavity cut in the common acrylic glass block. Pairs of quartz-glass windows in the opposite walls of each reaction cell enable continuous measurement of optical absorbance A_λ of the reaction mixture in the chosen cell. Mass exchange between adjacent cells occurs via connecting openings (*cf.* Figure 1). The intensity of mass exchange (coupling strength) is adjustable by means of vertically movable barriers controlling the cross-sectional area of the connecting openings. The reaction cell system can be operated either as a circular array of three cells or linear array of two or three cells. The intensity of mass exchange can be expressed by the value of the mass transport coefficient k_d determined in experiments with an inert tracer. The value of k_d equals the ratio of the volumetric flow rate between the adjacent cells to the volume of the cell. The value of the coefficient k_d is adjustable within the interval $0-0.025$ s^{-1}. The ratio of the intercell volumetric flow rate to the through-the-cell flow rate (*cf.* section 2.2) is therefore in the range $0-45$; that is, the region of high coupling strengths was mainly studied in our experiments compared, for example to the experiments of Crowley and Epstein.[12] The coupling between the cells was symmetric in all experimental cell arrangements due to equal volume of all cells in the array.

Platinum electrodes were used to measure the redox potential E_{Pt} in all cells (the calomel electrode was used as the reference one and the potentials were registered by a computer after AD conversion). No observable phase shift was detected between the time traces of E_{Pt} and A_{428} (absorbance at wavelength $\lambda =$ 428 nm corresponding to the absorption maximum of Ce^{4+} ions measured by means of the UV−vis HP-8452A spectrophotometer). The potentials E_{Pt} were therefore considered proportional to the concentration of Ce^{4+} ions in the BZ reaction mixture. The temperature inside the cells was measured by a thermistor and controlled by a water bath circulator.

The experiments on synchronization of oscillatory regimes were performed in the circular three-array of reaction cells. The intensity of the mass exchange was set to the same value for all pairs of adjacent cells. The experiments with the BZ reaction in the excitable regime were performed in the linear three-array of cells. The intensity of mass exchange was set to the same value both for the $1-2$ and the $2-3$ cell pairs.

2.2. Reaction Conditions. The four-bladed Rushton turbine type impellers (diameter 27 mm) were used for stirring; the controlled stirring speed was set to 350 min^{-1}. The mean residence time of the reaction mixture in all cells was 30 min in all experiments. The reactants were delivered in three separated streams into each reaction cell by means of a multichannel peristaltic pump; the inlet concentrations were the same in all cells. The reactant streams were preheated in a water bath before entering the reactor. All chemicals used in the experiments were of reagent grade.

TABLE 1: Values of Rate Constants and Other Parameters

parameter	oscillatory regime	excitable regime	unit
k_1	78.190	42.0	dm^6 mol^{-2} s^{-1}
k_{-1}	7.085×10^7	4.2×10^7	dm^3 mol^{-1} s^{-1}
k_3	2.910×10^5	8.0×10^4	dm^3 mol^{-1} s^{-1}
k_{-3}	13.89×10^3	8.9×10^3	dm^3 mol^{-1} s^{-1}
k_4	4.022×10^3	3.0×10^3	dm^3 mol^{-1} s^{-1}
k_5	2.710×10^6	3.0×10^6	dm^6 mol^{-2} s^{-1}
k_7	5.262	2.0	dm^6 mol^{-2} s^{-1}
k_8	1.334	0.4	dm^3 mol^{-1} s^{-1}
k_{13}	2.48×10^{-6}	0.0	s^{-1}
$k_{15}{}^a$		5.0×10^5	dm^3 mol^{-1} s^{-1}
$K_s{}^a$		7.7×10^{-13}	mol^2 dm^{-6}
A	0.08	0.3	mol dm^{-3}
B	0.05	0.1	mol dm^{-3}
h_0	3.02	0.82	mol dm^{-3}
z^0	0.002	0.006	mol dm^{-3}
k_0	5.556×10^{-4}	5.556×10^{-4}	s^{-1}

[a] *Cf.* Finkeová *et al.*[32] for values of k_{15} and K_s.

2.2.1. Oscillatory Regime. The inlet concentrations of reactants (related to cell volume) were $[Ce(SO_4)_2]_0 = 0.002$ mol dm^{-3}, $[H_2SO_4]_0 = 1.510$ mol dm^{-3}, $[CH_2(COOH)_2]_0 = 0.050$ mol dm^{-3}, and $[NaBrO_3]_0 = 0.080$ mol dm^{-3}. Reaction temperature was set to 35 ± 0.1 °C. The initial phase shifts among the oscillations in individual cells were adjusted by small additions of aqueous KBr solution, the value of the mass transfer coefficient k_d was varied systematically, and the time course of E_{Pt} in individual cells has been recorded.

2.2.2. Excitable Regime. The inlet concentrations of reactants (related to cell volume) were $[Ce(SO_4)_2]_0 = 0.006$ mol dm^{-3}, $[H_2SO_4]_0 = 0.410$ mol dm^{-3}, $[CH_2(COOH)_2]_0 = 0.100$ mol dm^{-3}, and $[NaBrO_3]_0 = 0.300$ mol dm^{-3}, and different values of inlet KBr concentrations ($[KBr]_0 = 0.004-0.100$ mol dm^{-3}) were used in order to change the threshold of excitability. The reaction temperature was set to 20 ± 0.1 °C.

The first cell was periodically stimulated by pulsed additions of a small volume ($10-60$ μL) of an aqueous solution of $AgNO_3$ (concentration 0.05 mol dm^{-3}). The added Ag^+ ions remove Br^- ions from the reaction mixture. The duration of a single pulse was about $0.1-0.4$ s. The number of moles of added Ag^+ ions divided by reaction cell volume V represents an amplitude A_S of the stimulation. The period T of periodic stimulations, the amplitude of stimulations A_S, and the mass transport coefficient k_d were varied systematically, and time courses of E_{Pt} in individual cells have been recorded.

3. Numerical Simulations

The dynamical behavior of the arrays of CSTRs was numerically simulated using the set of the mass balance equations for key reaction components

$$\frac{dc_{ij}}{d\tau} = f_{ij} + k_0 (c_{ij}^0 - c_{ij}) + k_d(c_{i,j-1} - 2c_{ij} + c_{i,j+1}) \quad (1)$$

where c_{ij} is molar concentration of component i in the jth cell; k_d is the mass transfer coefficient; k_0 is the reciprocal residence time in the single cell; $i = 1, ..., N$, where N is number of reaction components ($N = 4$ or $N = 5$, see below); and $j = 1, 2, 3$ denotes the index of the cell. Boundary conditions for eq 1 are (i) for the cyclic three-array $c_{i0} = c_{i3}$, $c_{i4} = c_{i1}$ and (ii) for the linear three-array $c_{i0} = c_{i1}$, $c_{i4} = c_{i3}$. Here we adopt the four-variable Oregonator based model[41] of the BZ reaction. Reaction rates f_{ij} in eq 1 are then given by

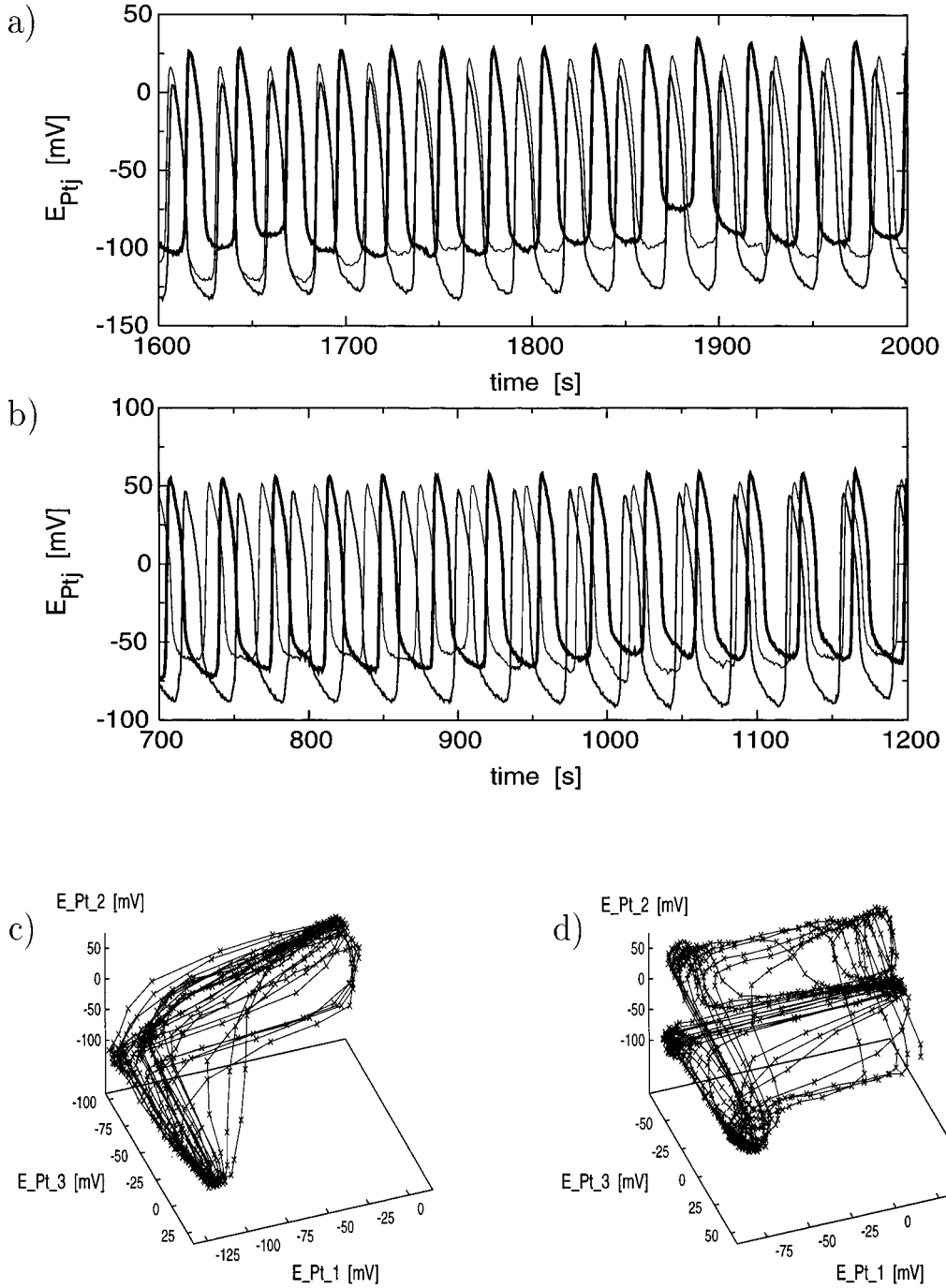

Figure 2. Experimental records of oscillatory modes in a circular three-array of reaction cells. (a) Two-in-phase regime, $k_d = 0.585 \times 10^{-3}$ s^{-1}. **(**b) synchronization of the all-out-of-phase regime, $k_d = 0.675 \times 10^{-3}$ s^{-1}. Thick line: cell 1, Medium line: cell 2. Thin line: cell 3. **(**c) Three-dimensional view of attractor for data in Figure 2a. **(**d) Three-dimensional view of attractor for data in Figure 2b.

$$f_{1j} = -r_{1j} + r_{-1,j} + r_{3j} - r_{-3,j} - 2r_{4j} - r_{5j} + r_{7j} \quad (2)$$

$$f_{2j} = -r_{5j} - r_{7j} + qr_{8j} + r_{13,j} \quad (3)$$

$$f_{3j} = 2(r_{1j} - r_{-1,j}) - r_{3j} + r_{-3,j} \quad (4)$$

$$f_{4j} = r_{3j} - r_{-3,j} - r_{8j} \quad (5)$$

This set of equations describes reaction rates when no Ag^+ ions are present ($N = 4$). When Ag^+ ions are added to the reaction mixture, the kinetics and equilibrium of their precipitation with Br^- ions have to be considered ($N = 5$). Equation 3 is then in the form

$$f_{2j} = -r_{5j} - r_{7j} + qr_{8j} + r_{13,j} + r_{15,j} \quad (3a)$$

and the equation

$$f_{5j} = r_{15,j} \quad (6)$$

is added to the set of eqs 2−5. The reaction rates on the right-hand sides of eqs 2−6 are

$$r_{1j} = k_1 h_0 A x_j \qquad r_{-1,j} = k_{-1} u_j^2 \qquad r_{3j} = k_3 u_j (z_j^0 - z_j)$$
$$r_{-3,j} = k_{-3} x_j z_j \qquad r_{4j} = k_4 x_j^2 \qquad r_{5j} = k_5 h_0 x_j y_j$$
$$r_{7j} = k_7 h_0 A y_j \qquad r_{8j} = k_8 B z_j \qquad r_{13,j} = k_{13} B$$
$$r_{15,j} = k_{15}(K_s - y_j s_j)$$

Here $x_j \equiv c_{1j}$, $y_j \equiv c_{2j}$, $u_j \equiv c_{3j}$, $z_j \equiv c_{4j}$, and $s_j \equiv c_{5j}$ are the jth cell concentrations of reaction components $HBrO_2$, Br^-, $HBrO_2^+$, Ce^{4+}, and Ag^+, respectively. The values of rate constants and other parameters used for modeling of both the oscillatory and the excitable regime of the BZ reaction are given in Table 1 (K_s denotes the solubility product of AgBr, h_0 is the Hammett acidity function[42]).

In order to examine the stability of the phase-shifted oscillatory modes (*cf.* next paragraph) under the random fluctuations of the coupling strength among the cells due to hydrodynamic fluctuations of the liquid flow inside the channels connecting the cells, the coupling strength coefficient k_d was modeled as a correlated γ-distributed stochastic process. The Langevin stochastic differential equation (SDE),[47]

$$dk_d = (\alpha - \beta k_d)\, dt + \sqrt{2\delta k_d}\, dW(t) \qquad (7)$$

was used for the simulation of the temporal evolution of k_d. In eq 7 α, β, and δ are non-negative constants and $W(t)$ is the Wiener process.[47] The stochastic process generated by eq 7 has a mean value $\bar{k}_d = \alpha/\beta$ and a correlation function

$$R_{k_d}(\tau) = \frac{\alpha\delta}{\beta^2}\exp(-\beta\tau) + \left(\frac{\alpha}{\beta}\right)^2 \qquad (8)$$

The variance to mean ratio is equal to δ/β. Equation 7 was solved numerically[48,49] simultaneously with the balance equations (1).

4. Results and Discussion

4.1. Oscillatory Regime. Three particular oscillatory modes were examined in experiments: (i) all-out-of-phase mode (rotating phase wave, the AOP mode), (ii) two-in-phase mode (the TIP mode), and (iii) all-in-phase mode (the AIP mode). Oscillations in all reaction cells are mutually shifted by one-third of the period at the AOP regime; in the case of the TIP mode the oscillations in two cells are phase synchronized and the third cell oscillations are phase shifted by half of the period. The oscillations in all cells are phase synchronized in the case of the AIP mode. The AIP mode represents the stable oscillatory regime in the circular array of CSTRs. No spontaneous desynchronization of the AIP mode was detected in experiments at all values of the coupling strength coefficient. Only small temporary phase shifts were observed at very low values of the coupling strength coefficient ($k_d \leq 0.001\ s^{-1}$). These small shifts occurred due to small irregular fluctuations of the period of oscillations in individual cells. The TIP mode (see Figures 2a,c and 3a) was observed to be stable only at low k_d values (approximately within the interval $0-0.01\ s^{-1}$). The time traces of Pt-electrode potentials in Figure 2a and the phase shifts in Figure 3a exhibit variations of both amplitude and the period of the oscillations due to fluctuations of the coupling strength caused by hydrodynamic fluctuations within the openings connecting the cells. The pronounced sensitivity of the BZ reaction to effects of the imperfect stirring is a well-known experimental fact (see, for example, refs 45 and 46). This sensitivity is reflected in enhanced instability of the AOP mode observed in experiments (*cf.* Figures 2b,d and 3b,c, where gradual synchronization and desynchronization, respectively, of the AOP mode are shown). The AOP mode in the experiments was detected only over relatively short time intervals (about 20 oscillations). The stable phase-shifted modes were observed in experiments by Yoshimoto *et al.*,[20] however, in the coupled cell system with asymetric active coupling via peristaltic pumping where the fluctuations of the coupling strength are minimized.

Figure 4 shows results of numerical simulations of synchronization phenomena in the circular three-array of reaction cells as a function of the coupling strength coefficient k_d. The set of eqs 1−5 was used with parameter values in Table 1 (oscillatory regime). The AOP mode was used as the initial state in Figure 4a,c; the TIP mode was used in Figure 4b,d. The coupling strength coefficient k_d was then gradually increased from zero in a stepwise manner (transients were discarded at each particular k_d value). The phase shift of the unsynchronized cell varies significantly with the increasing coupling strength in the case of the partly symmetric initial state TIP (see Figure 4b); the observed solution moves away from the TIP mode, and a fully asymmetric solution with uneven phase shifts temporarily arises. However, abrupt synchronization of oscillations in all cells occurs at $k_d = 0.01374\ s^{-1}$. The synchronization is very fast: the oscillations in all cells synchronize within several oscillations. The same phenomenon was observed by Somers and Kopell,[44] who performed a theoretical study of synchronizations in arrays of both phase and relaxational oscillators. The symmetric AOP state (see Figure 4a)—the rotating phase-wave solution—is stable over a wide range of values of the coupling coefficient ($k_d \leq 0.008\ 05\ s^{-1}$). Then at $k_d = 0.00805\ s^{-1}$ two cells synchronize spontaneously and the TIP mode is established. The phase shift of the unsynchronized cell slightly varies when the coupling strength is further increased, and eventually, at $k_d = 0.013\ 74\ s^{-1}$ the fully synchronized AIP mode is reached. The periods of oscillations in all reaction cells change simultaneously with the phase shifts (*cf.* Figure 4c,d). The periods increase with the increasing coupling strength; a steep increase occurs when the k_d value approaches the synchronization point, which was observed also

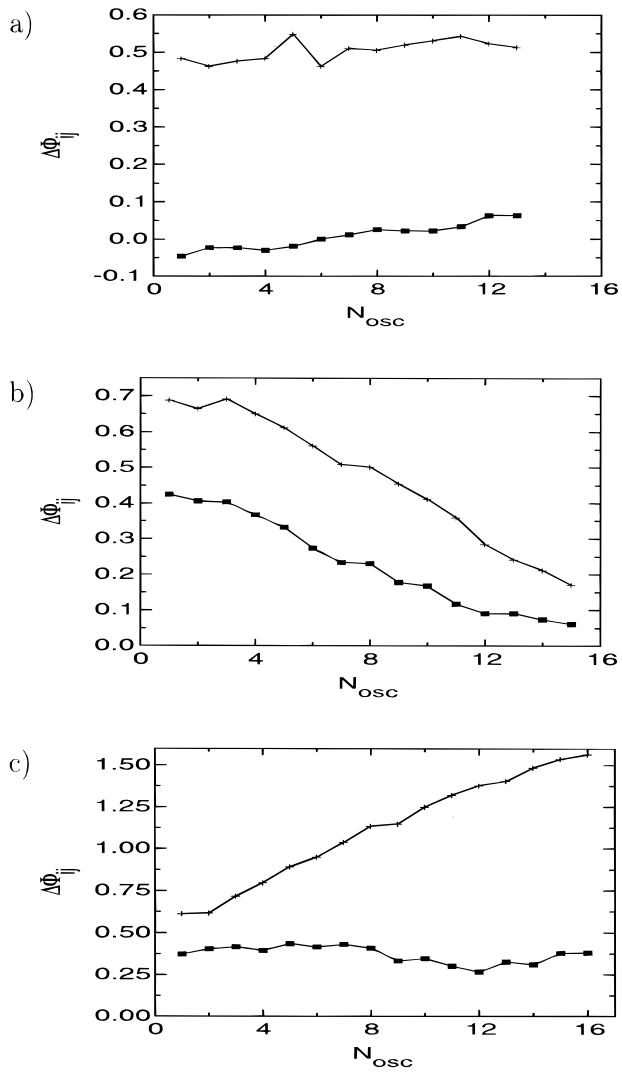

Figure 3. Phase shifts of the oscillatory modes shown in Figure 2. (a) Two-in-phase regime (*cf.* Figure 2a). (b) Synchronization of the all-out-of-phase regime (*cf.* Figure 2b). (c) Desynchronization of the all-out-of-phase regime (*cf.* Figure 2c). Phase shifts are related to oscillations in cell 1 (*i.e.*, $\Delta\Phi_{11} = 0.0$, not plotted): (+) phase shift $\Delta\Phi_{21}$ of the cell 2, (■) phase shift $\Delta\Phi_{31}$ of the cell 3.

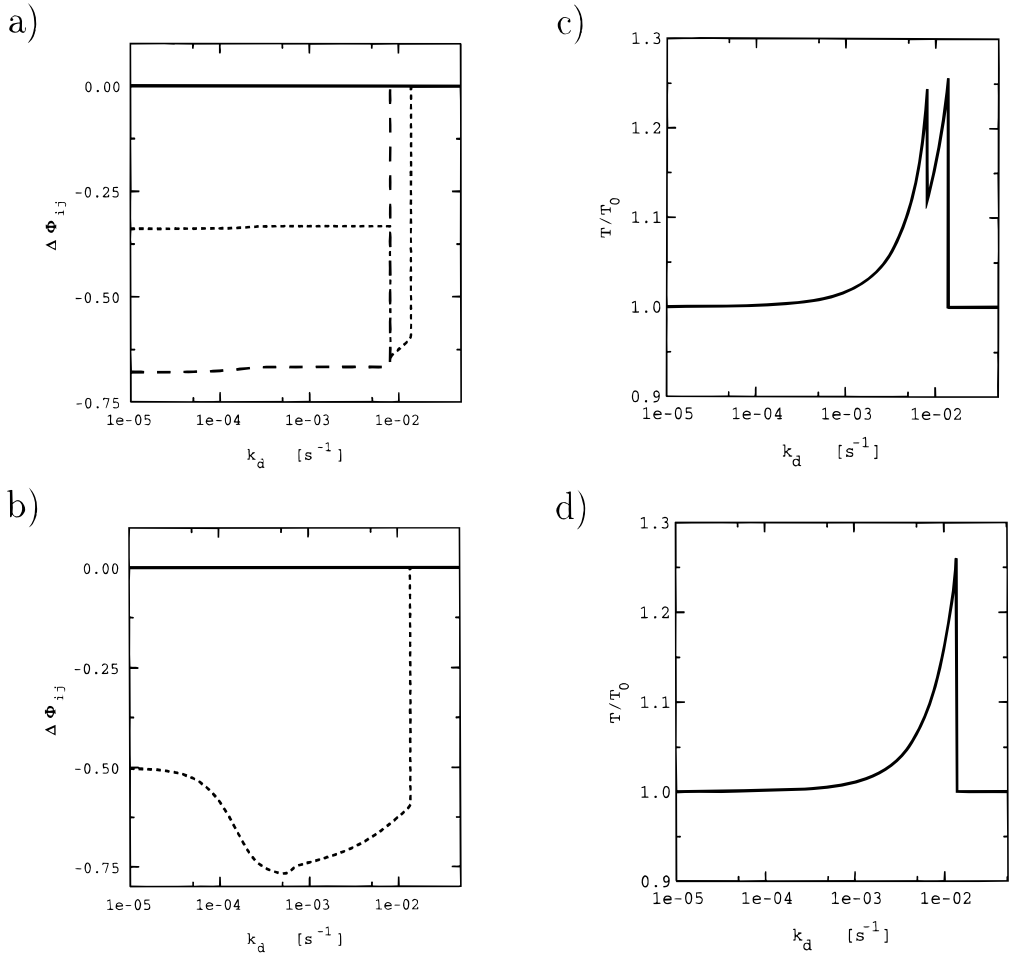

Figure 4. Numerical simulation of synchronization of oscillations in reaction cells. (a, b) Phase shifts $\Delta\Phi_{ij}$ as function of the coupling strength; (a) AOP initial state, (b) TIP initial state). (c, d) Scaled period T/T_0 of oscillations as a function of the coupling strength k_d; (c) AOP initial state, (d) TIP initial state). (—) Cell 1 (the reference cell), (- - -) cell 2, (— — —) cell 3. The lines for cells 1 and 3 coincide in part b.

by Crowley and Epstein.[12] At the synchronization point the value of the period returns to its initial (autonomous) value.

The spontaneous synchronization of the TIP and AOP modes caused by stochastic fluctuations of the coupling coefficient k_d is shown in Figure 5, where numerically simulated Ce^{4+} concentrations in individual cells are plotted in the phase plane $z_i - z_j$ ($i, j = 1, 2, 3$). The TIP and AOP modes (used as the initial conditions) are stable in the absence of the noise (Figure 5a,c); when the noise is applied, a fast transition to the synchronized AIP mode occurs (Figure 5b,d). These results are in agreement with our experimental observations of a weak stability of the phase-shifted modes (TIP and AOP), which is likely due to fluctuations of the coupling strength in the coupled cell systems with a noisy direct mass-flow coupling.

The experimental observations and the results of numerical simulations of the oscillatory regimes in the cyclic three-array of reaction cells are in general agreement. Both of them exhibit the same oscillatory regimes and the phenomena of their synchronization. There is however a difference in time scaling; that is, the values of the periods of simulated oscillatory regimes do not match precisely their experimental values. No stable stationary state patterns within the cell array were detected in either experiments or simulations.

4.2. Excitable Regime. The observed regimes of propagating excitation in the linear *n*-array of coupled excitators exposed to periodic external stimulations of the first cell are characterized by their values of a firing vector $\sigma = \{\sigma_j, j = 1, ..., n\}$, which is composed of individual firing numbers σ_j defined as

$$\sigma_j = P_j/Q_1 \qquad (9)$$

where P_j is the number of excitations in the jth cell and Q_1 is the number of stimulations applied in the first cell within a long time interval.

The excitability level of the BZ reaction mixture is indirectly proportional to Br^- concentration. The BZ mixture described in section 2.2.2 oscillates autonomously under given reaction conditions and at zero or very low Br^- concentrations. The minimum inlet Br^- concentration necessary for the suppression of the oscillations was found to be $y^0 = 0.004$ mol dm^{-3}, and the threshold of the excitability in a single reaction cell was $A_{S_{th}} \approx 1.0 \times 10^{-5}$ mol dm^{-3} at that inlet Br^- concentration. The value of $A_{S_{th}}$ increases in an almost linear way with the increasing y^0 value: at $y^0 = 0.010$ mol dm^{-3} the threshold of the excitability is $A_{S_{th}} \approx 6.0 \times 10^{-5}$ mol dm^{-3}. Thus the level of the excitability can be easily adjusted by the choice of y^0.

Classification of excitation regimes observed in the linear array of three coupled reaction cells adopted in this paper is, in principle, based on that used by Kosek *et al.*[43] for the two-cell system. We classify the observed excitation regimes according to the extent of excitation propagation. The following classes can be found (assuming $\sigma_1 > 0$).

(a) Complete Propagation. Each excitation in the first cell propagates to both the second and the third cells, *i.e.*, $\sigma_2/\sigma_1 = \sigma_3/\sigma_1 = 1$. Two subclasses of this propagation regime can be defined: (a_1) *complete propagation of every stimulation, i.e.* $\sigma_1 = \sigma_2 = \sigma_3 = 1$, and ($a_2$) *complete propagation of every excitation, i.e.* $\sigma_1 = \sigma_2 = \sigma_3 < 1$.

(b) Partial Propagation. This is characterized by firing numbers $0 < \sigma_2/\sigma_1 < 1$ and $0 < \sigma_3/\sigma_1 < 1$. This class can be further divided into two subclasses: (b_1) *synchronized partial*

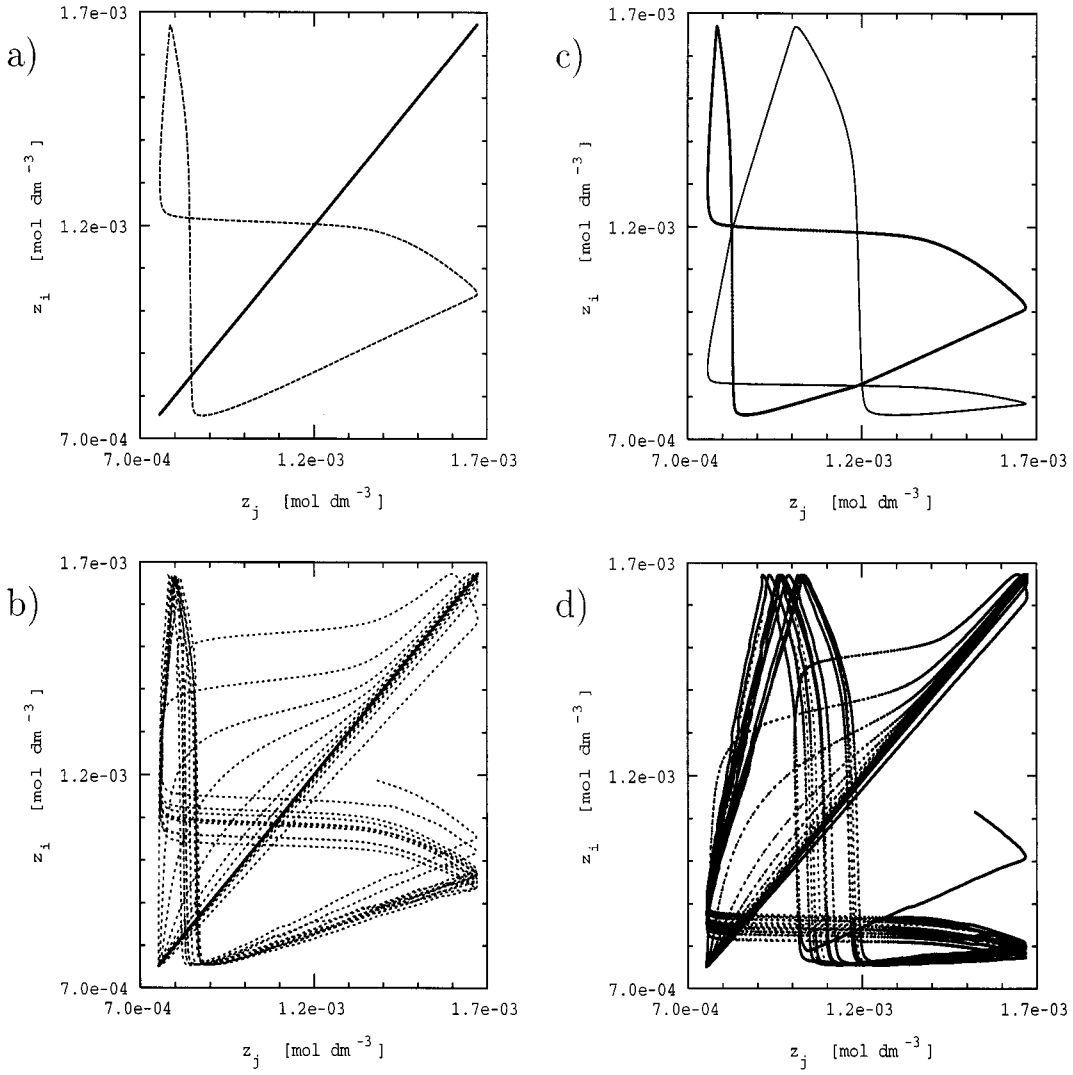

Figure 5. Numerical simulations of the effects of stochastic fluctuations of the coupling strength coefficient k_d on synchronization of the TIP mode (a, b) and the AOP mode (c, d). (a and c) No noise applied; (b and d) noise applied; variance to mean ratio 0.9%; mean value $\bar{k}_d = 0.006\ s^{-1}$. Parameters in eq 7: $\alpha = 0.06\ s^{-2}$, $\beta = 10.0\ s^{-1}$, $\delta = 0.09\ s^{-2}$. Full line: cells 1 and 2. Dashed line: cells 2 and 3.

propagation, characterized by the same values of the firing numbers in the cells 2 and 3, *i.e.*, $\sigma_2 = \sigma_3$, and (*b*$_2$) *unsynchronized partial propagation*, with different values of the firing numbers in the nonstimulated cells, *i.e.*, $\sigma_2 \neq \sigma_3$.

(*c*) *Partial Propagation Failure*. There is no excitation in the third cell, *i.e.*, $\sigma_3 = 0$ with $0 < \sigma_1 \leq 1$ and $0 < \sigma_2 \leq 1$.

(*d*) *Complete Propagation Failure*. There are no excitations in both nonstimulated cells, *i.e.*, $\sigma_2 = \sigma_3 = 0$.

Examples of particular excitation regimes indicated by the potentials of the Pt electrodes in all reaction cells are shown in Figure 6. A complete propagation of the excitation with the firing vector (1,1,1) is shown in Figure 6a for the stimulation period $T = 120$ s. A synchronized partial propagation regime with the firing vector (1, $^1/_2$, $^1/_2$) at the forcing period $T = 70$ s is recorded in Figure 6b. Figure 6c shows a partial propagation failure pattern with the firing vector (1,1,0).

A complete overview of both the experimentally observed and numerically simulated excitation regimes in the linear three-array of coupled cells is given in Figures 7−11. The values of rate constants and other parameters in Table 1 (excitable regime) were used for numerical simulations.

The phase diagrams in Figures 7a and 8a show the experimentally observed occurrence of the particular excitation regimes in the A_S-T plane at a fixed value of the coupling strength coefficient k_d and two values of inlet Br^- concentrations, *i.e.* at two different thresholds of the excitability. The complete propagation regime with the firing vector (1,1,1) is possible only at sufficiently high perturbation amplitude A_S and long perturbation period T. Partial propagation regimes begin to appear with decreasing values of T. Firing numbers σ_i in all cells generally decrease with the decrease of both the amplitude and the period of perturbations. Complete propagation regimes with the firing vectors ($\sigma_1 = \sigma_2 = \sigma_3$, $\sigma_i < 1$) prevail at lower values of the stimulation amplitude (*ca.* below $A_S = 4.5 \times 10^{-5}$ mol dm^{-3}). Mainly synchronized partial propagation regimes, characterized by firing numbers $\sigma_2 = \sigma_3 = {}^1/_2\sigma_1$, are observed above this limit. Windows of the complete propagation failure were detected at values of A_S larger than about 4×10^{-5} mol dm^{-3}. The richness of experimentally detected and numerically simulated regimes decreases with the increasing value of the inlet Br^- concentration y^0, *i.e.* with the increasing threshold of the excitability. Only three regimes were observed in experiments at $y^0 = 0.010$ mol dm^{-3}: no excitations in either cell, $\sigma_I = (0,0,0)$, and two complete propagation failure regimes, $\sigma_{II} = ({}^1/_2,0,0)$ and $\sigma_{III} = (1,0,0)$ (results not shown in figures). The first regime occurs below the excitability threshold, the second one at the forcing period $T \leq 50$ s, and the last one at the forcing period $T > 50$ s. No unsynchronized partial propagations and partial propagation failures were observed except for the excitation regime with the firing vector (1,1,$^1/_2$) in Figure 8a at high A_S and long T. Typically, each time the second cell is excited the third cell is also excited. Hence the linear three-

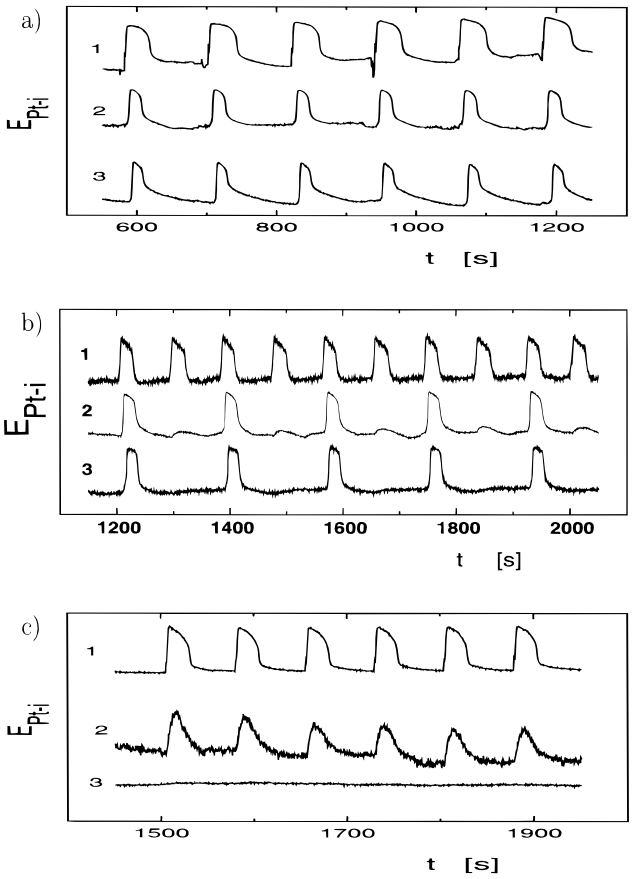

Figure 6. Examples of experimentally observed time records of potentials of platinum electrodes (plotted in arbitrary units) in a linear three-array of coupled CSTRs. Periodic stimulations of the first cell: (a) 1:1:1 regime (full propagation of excitations); (b) 1:$^1/_2$:$^1/_2$ regime (partial propagation of excitations); (c) 1:1:0 regime (partial propagation failure). Parameters: $k_d = 2.247 \times 10^{-2}$ s^{-1}, $A_S = 6.67 \times 10^{-5}$ mol dm^{-3}, $y^0 = 0.004$ mol dm^{-3}.

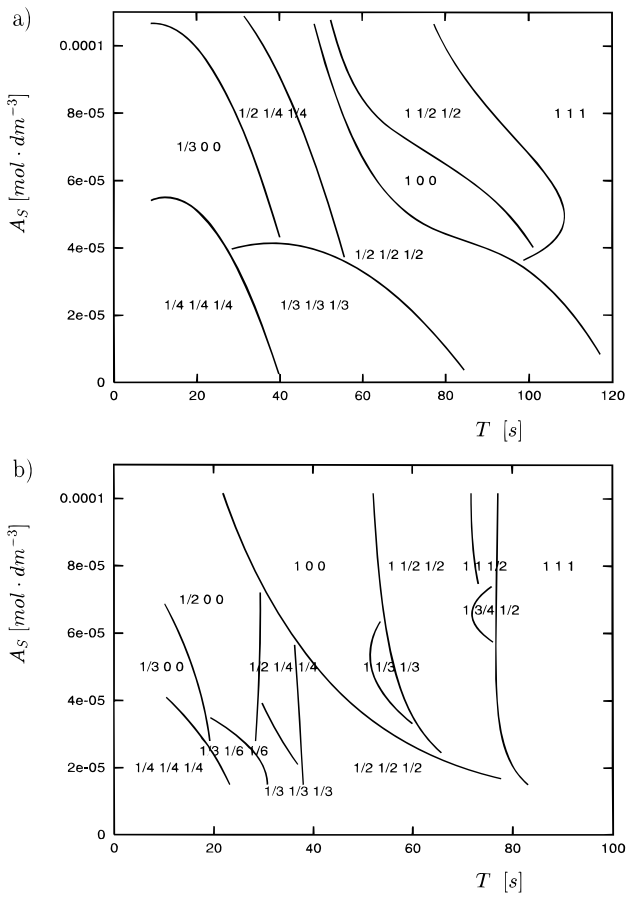

Figure 7. Period−amplitude phase diagram for higher excitability level constructed from experimental (**a**) and simulated (**b**) data; the value of the firing vector $\sigma = (\sigma_1, \sigma_2, \sigma_3)$ defines a partition of the parameter plane into regions with particular dynamic modes. Parameters: $k_d = 2.247 \times 10^{-2}$ s^{-1}, $y^0 = 0.004$ mol dm^{-3}.

array of excitable cells mimics the behavior of the two-cell system. This observation can be extended to linear arrays with four and more cells with equal coupling strengths: if the excitation is transferred from the perturbed cell to the adjacent one, it tends to propagate along the array like a pulse wave.

The plots of the firing vector $\sigma = (\sigma_1,\sigma_2,\sigma_3)$ versus the perturbation period T or the stimulus amplitude A_S are called excitation diagrams; they typically form devil's staircase-like structures.[50] Excitation diagrams corresponding to selected values of A_S and T in Figures 7a (lower threshold of the excitability) and 8a (higher threshold of the excitability) are shown in Figures 10 and 11.

The experimentally observed effects of the decreasing stimulus amplitude on the observed excitation patterns are shown in Figure 10a-c. The regimes of complete excitation propagation occur at low and intermediate perturbation amplitudes, whereas at high A_S both partial propagation and complete propagation failure regimes occur; that is, the overstimulation in the first cell hinders the spreading of the excitation along the array. The evolution of the excitation regimes with the increasing perturbation amplitude A_S at fixed $T = 60$ s is shown in Figure 10d. The propagation of the excitations from the stimulated cell to the second and third ones begins to fail at $A_S \approx 6.0 \times 10^{-5}$mol dm^{-3}. The window of the complete propagation failure regime with the firing vector (1,0,0) is located above this value and is followed by the partial propagation regime with the firing vector (1,$^1/_2$,$^1/_2$). The excitation diagrams in Figures 10a,b and 11a,b allow for comparison of excitation patterns at two excitability levels: the partial propagation and complete propagation regimes are enhanced by suppressed excitability level. Decreasing the value of the coupling strength coefficient k_d has the same effects on the observed excitation patterns as shown in Figure 11b,c,d.

All cells in the array synchronize at lower stimulus amplitude; that is, only complete propagation regimes exist. Individual excitation regimes move toward longer stimulation periods at increased excitability level (*cf.* Figure 10b,c). The synchronization of the excitation regimes ceases to exist at either decreased excitability level or decreased coupling strength (see Figure 11).

Hierarchical evolution of the partial propagation excitation regimes together with the occurrence of the propagation failure as a function of the stimulus period is shown in Figure 10a. At high stimulus amplitudes, the first cell fires at every third stimulus, *i.e.* $\sigma_1 = {}^1/_3$. The excitations do not propagate until the stimulus period exceeds the value of 35 s. Then the firing number in the first cell increases to $\sigma_1 = {}^1/_2$, and the second and the third cells begin to excite with the firing numbers being half of σ_1, *i.e.* $\sigma_2 = \sigma_3 = {}^1/_4$. The propagation failure regime is then reestablished within the interval of the stimulus periods 60 s $\le T \le$ 75 s. The complete propagation failure occurs at sufficiently high amplitudes of stimulation A_S and/or at low coupling strengths. The partial propagation regime with $\sigma =$ (1,$^1/_2$,$^1/_2$) is established at $T >$ 75 s (see Figure 10a); this regime eventually ($T \ge 120$ s) undergoes a transition to the complete propagation through all cells, *i.e.* $\sigma = (1,1,1)$. A similar scenario of the development of the excitation patterns can be also seen in Figure 11a,b,c,d. The occurrence of the phenomenon of the complete or partial propagation failure is also closely related to the refractory time of the excitable BZ reaction. The first cell in the array cannot respond to a new stimulus until it recovers from the previous excitation. This fact is clearly observable in Figures 10 and 11, where the firing number $\sigma_1 =$

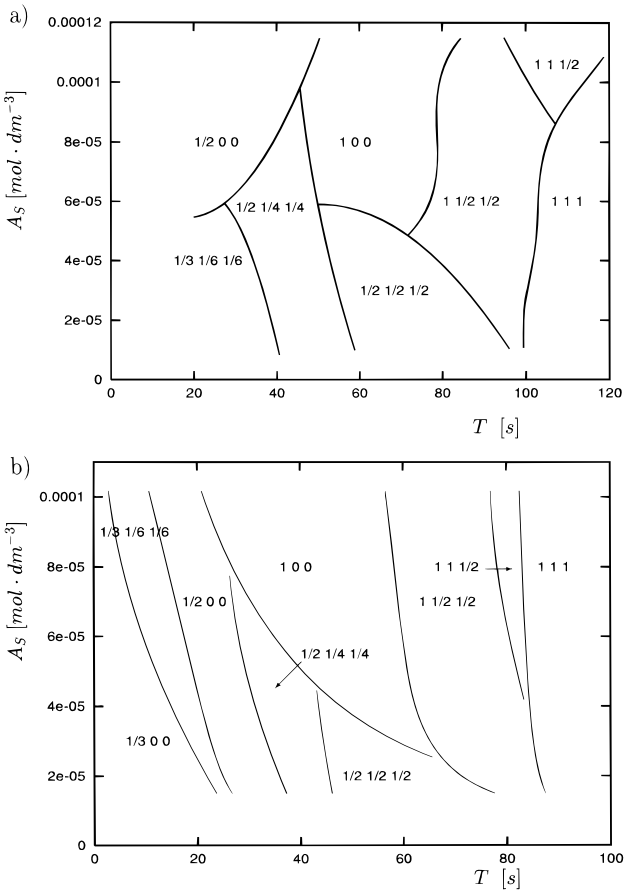

Figure 8. Period−amplitude phase diagram for lower excitability level constructed from experimental (**a**) and simulated (**b**) data. Parameters: $k_d = 2.247 \times 10^{-2}$ s^{-1}, $y^0 = 0.006$ mol dm^{-3}.

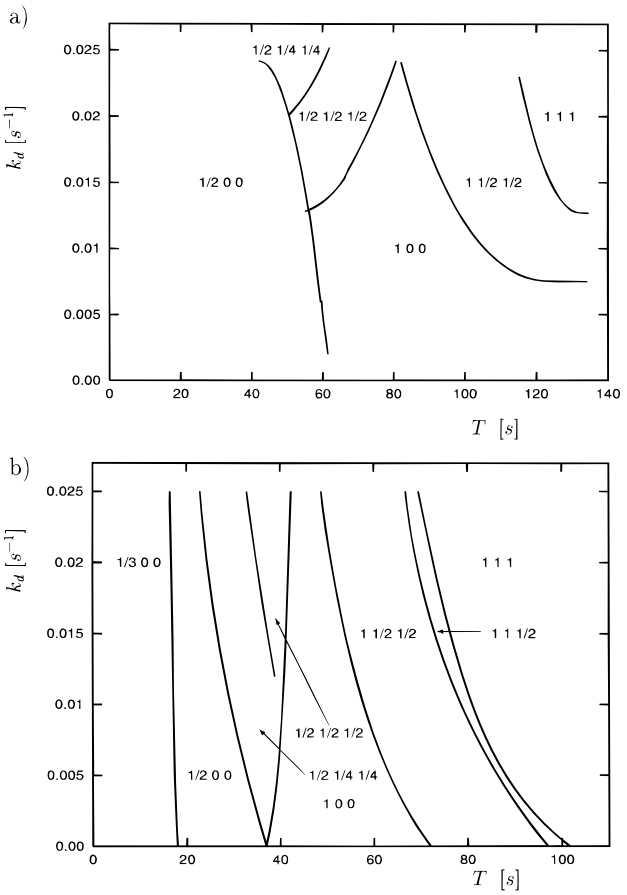

Figure 9. Period−coupling strength phase diagram for higher excitability level constructed from experimental (**a**) and simulated (**b**) data. Parameters: $A_S = 3.3 \times 10^{-5}$ mol dm^{-3}, $y^0 = 0.004$ mol dm^{-3}.

0 at short stimulus periods. Even if the first cell excites after the external stimulus, the second and the third cells may not fire due to increased excitability threshold value during the refractory period (*cf.* Figure 9 in the paper by Kosek and Marek,[35] where the phase space structure around the excitable stable node of the BZ reaction is shown). The second and the third cells can excite again only when the system trajectory approaches the close vicinity of the stationary state.

The structure of the numerically simulated excitation diagrams in Figures 7b and 8b essentially reproduce the structure of the diagrams constructed from experimental observations. However, the regions occupied by corresponding excitation regimes differ in size and in their relative position within the diagram plane. For the most part, these differences are due to different time scaling of the kinetic model and the experiments. Moreover, numerically simulated diagrams involve small regions with firing vectors (1,1,$^1/_2$) and (1,$^3/_4$,$^1/_2$) corresponding to unsynchronized partial propagation regimes not observed in experiments. This discrepancy probably arises due to lowered stability of the unsynchronized partial propagation regimes in the experimental system with the fluctuating coupling strength among the reaction cells. The regions of the parametric plane occupied with these regimes are, moreover, very small and therefore are hard to detect in experiments where a relatively course grid of the experimental points can be used.

The occurrence of distinct excitation regimes in the parametric plane k_d-T at fixed A_S and y^0 values (intermediate stimulation amplitude, low threshold of excitability) is depicted in Figure 9, part a (experimental results) and b (simulation results). The complete propagation failure regimes with the firing vectors ($^1/_2$,0,0) and (1,0,0) dominate in the diagram constructed from the experimental observations. No propagation of the excitations occurs at $A_S \leq 1.25 \times 10^{-5}$ mol dm^{-3} except for quite long stimulation periods ($T > 120$ s). The limiting A_S value agrees well with the excitability threshold value. The partial and complete propagation regimes observed at higher values of T and k_d are separated by a region of complete propagation failure with $\sigma = (1,0,0)$. The simulation results in Figure 9b again qualitatively correspond to the experimental ones. Only two excitation regimes detected in simulations, namely, those with $\sigma = (^1/_3,0,0)$ and $\sigma = (1,1,^1/_2)$, were not observed in experiments. Simulations, however, do predict the existence of both complete and partial propagation regimes even at very low coupling strengths (see narrow regions corresponding to these regimes in Figure 10). It can be expected that the character of mass transfer among the cells in experiments is changing with the decreasing coupling strength; the transfer of the excitation from the excited cell to the nonexcited one can be delayed due to a different hydrodynamic flow. In such a case the perturbation would no longer be pulselike but distributed in time at sufficiently low coupling strengths. This effect can result in failed excitations observed in experiments.

5. Conclusions

Experimental and numerical studies of oscillatory regimes in the cyclic three-array of mass exchange coupled continuous stirred tank reactors with the BZ reaction point to generic behavior of chemical oscillators cyclically coupled via mutual mass exchange. Experiments show strong stability of fully synchronized in-phase oscillatory regimes over the entire range of the experimentally accessible values of the coupling strength coefficient and a limited stability of the phase-shifted oscillatory regimes occurring only in a narrow interval of the lowest values of the coupling strength coefficient. Numerical simulations

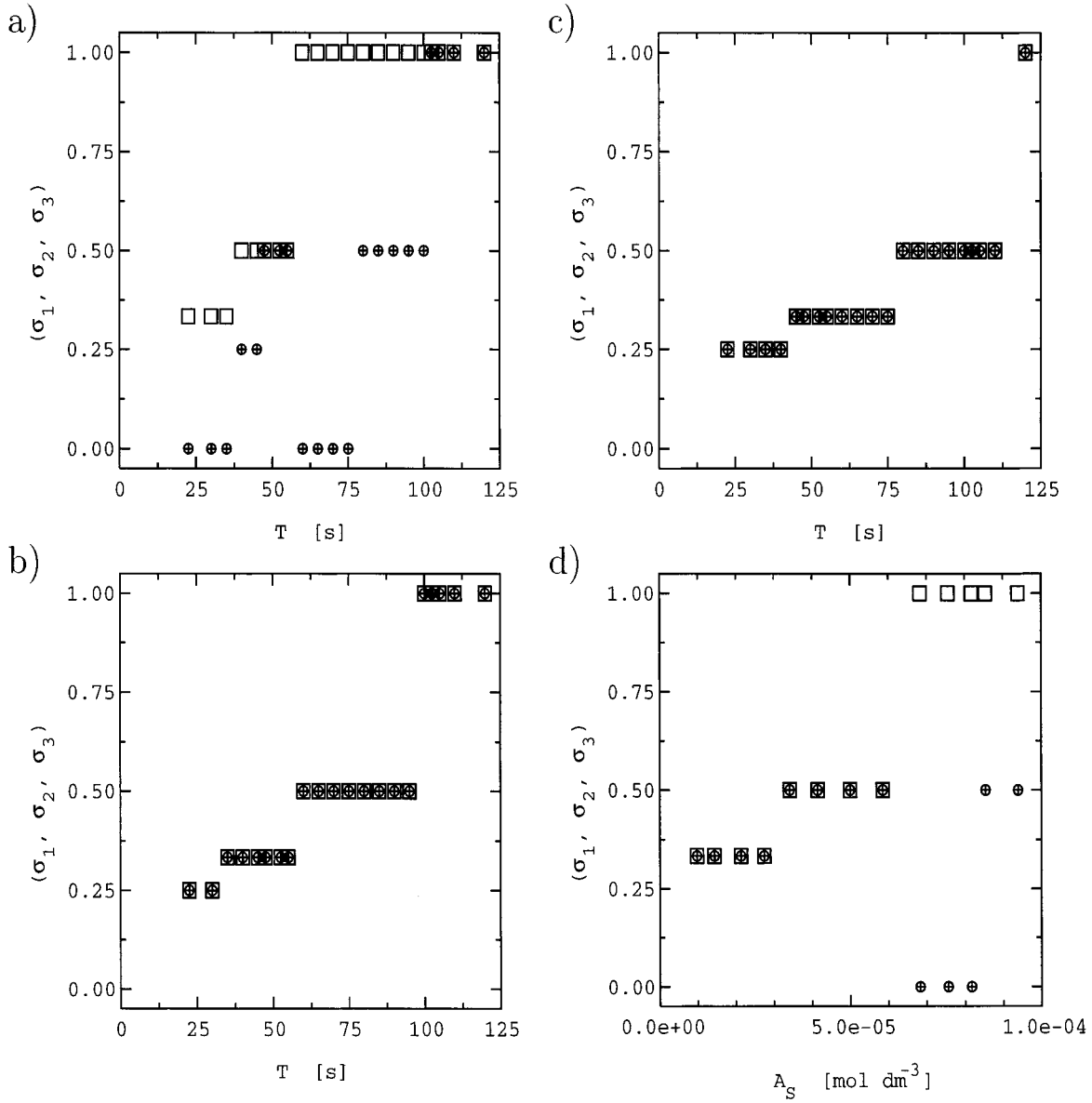

Figure 10. Plot of the firing vector (σ_1,σ_2,σ_3) versus T constructed from experiments (*cf.* Figure 7): (□) cell 1; (○) cell 2; (+) cell 3. Parameters: $k_d = 2.247 \times 10^{-2}$ s^{-1}, $y^0 = 0.004$ mol dm^{-3}; (a) $A_S = 6.67 \times 10^{-5}$ mol dm^{-3}; (b) $A_S = 2.88 \times 10^{-5}$ mol dm^{-3}; (c) $A_S = 1.46 \times 10^{-5}$ mol dm^{-3}; (d) $T = 60.0$ s.

using a four-variable Oregonator based model of the BZ reaction yield qualitatively concordant results: under the increasing coupling strength the original evenly phase-shifted oscillations in individual reactors first abruptly synchronize to a partially synchronized oscillatory regime (two-in-phase mode), and eventually, a second abrupt transition to a fully synchronized regime (all-in-phase mode) occurs. The experiments demonstrate fast spontaneous randomly occurring transitions of the phase-shifted oscillatory regimes to the synchronized all-in-phase regime when the coupling among the reactors is kept constant within the region of the existence of stable phase-shifted oscillatory regimes. These observations are reproduced by numerical simulations with the coupling strength fluctuating randomly around a prescribed constant mean value. The same spontaneous transitions as in experiments were found at reasonably low level of the coupling strength variations (variance to mean ratio 0.9%). A detailed numerical study of oscillatory regimes in various circular arrays of chemical oscillators employing continuation techniques is in progress. The experimental and simulation results indicate that the intensity of mutual coupling in the direct mass exchange coupled (bio-)chemical oscillator systems plays a dominant role in situations where precisely set phase shifts among individual oscillators are crucial, for example in the case of cell−cell communication. Strong coupling or low levels of random coupling strength fluctuations can either totally destroy or at least seriously damage the required phase-shifted oscillatory regime.

The results of both experimental and numerical studies of the excitatory patterns in the linear three-array of equally coupled BZ excitators with periodic pulsed perturbations display a full range of particular excitatory patterns: the complete propagation, the partial propagation (both synchronized and unsynchronized), and full and partial propagation failure. In general, the excitatory patterns in the system tend to the complete propagation of excitations with the firing vector (1,1,1) at high coupling intensity, long perturbation period, and high stimulus amplitude. When the value of either of these parameters is lowered, both complete propagation regimes with the firing vectors ($\sigma_1 < 1$, $\sigma_2 = \sigma_1$, $\sigma_3 = \sigma_1$) and partial excitation propagation regimes with the firing vectors ($\sigma_1 \leq 1$, $\sigma_2 < \sigma_1$, $\sigma_3 < \sigma_1$) begin to emerge. The values of firing numbers in individual reactors decrease when the values of the control parameters are lowered, and eventually the firings cease at very low stimulus amplitude (close to the excitability threshold) or very short stimulation period. The transfer of the excitation from the first to the second cell fails at weak coupling strengths;

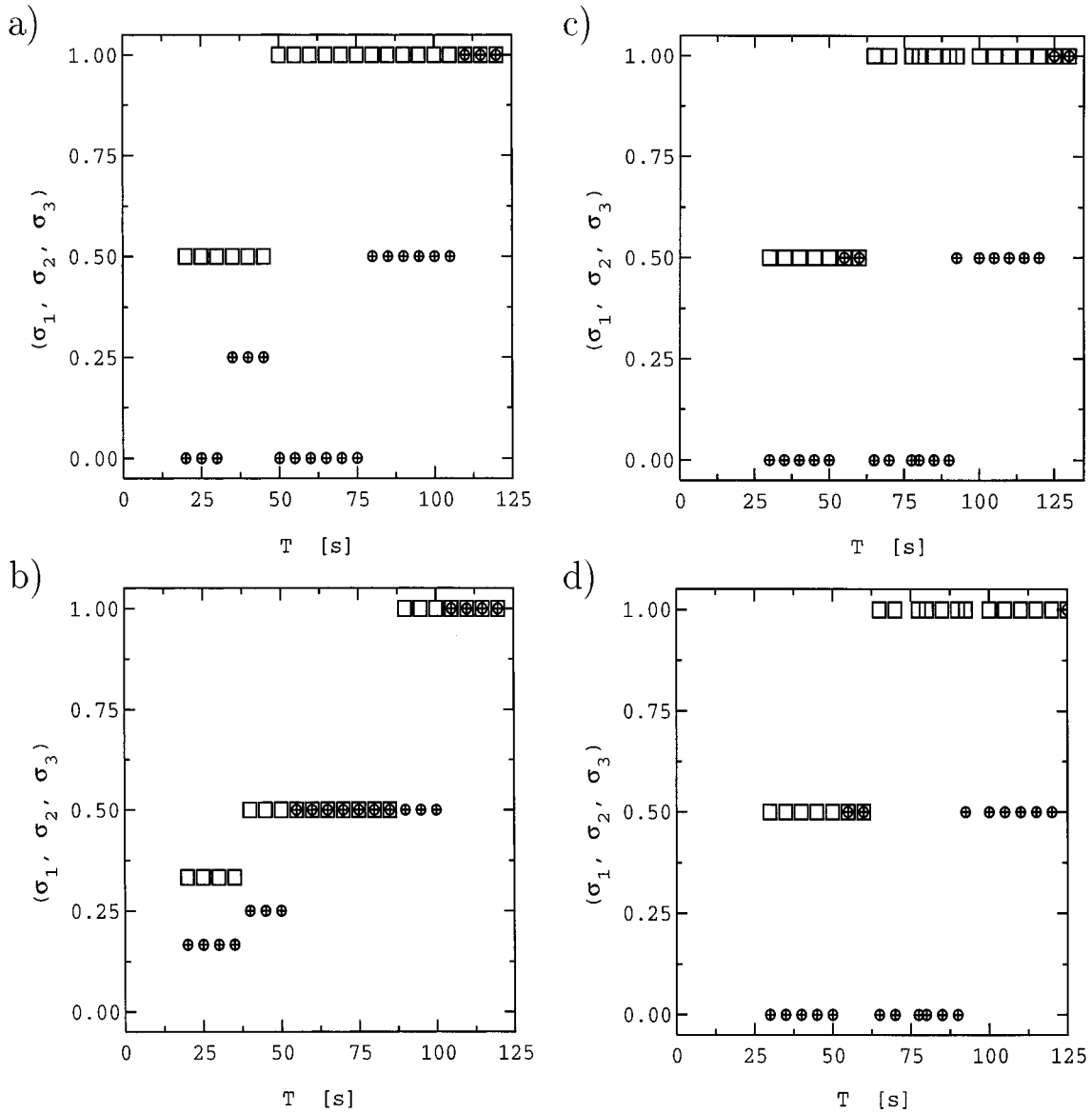

Figure 11. Plot of the firing vector (σ_1,σ_2,σ_3) versus T constructed from experiments (*cf.* Figures 8 and 9): and (□) cell 1; (○) cell 2; (+) cell 3. Parameters: $y^0 = 0.006$ mol dm^{-3}; (a) $A_S = 6.67 \times 10^{-5}$ mol dm^{-3}, $k_d = 2.247 \times 10^{-2}$ s^{-1}; **(**b) $A_S = 3.33 \times 10^{-5}$ mol dm^{-3} ;$k_d = 2.247 \times 10^{-2}$ s^{-1}; (c) $k_d = 1.50 \times 10^{-2}$ s^{-1}; $A_S = 3.33 \times 10^{-5}$ mol dm^{-3}; (d) $k_d = 1.00 \times 10^{-2}$ s^{-1}; $A_S = 3.33 \times 10^{-5}$ mol dm^{-3}.

that is, the complete propagation failure pattern prevails within the region of weak coupling in the parametric space. Detailed calculations show that the regions of the occurrence of the excitatory patterns characterized by particular values of the excitation vector are ordered in a highly complex manner within the parametric phase plane with possible overlappings (a multiplicity of the excitatory patterns). However, only the most stable excitatory patterns are detected both in experiments and numerical simulations with added noise. The occurrence of the complete and/or partial propagation failure patterns is manifested both in experimental results and numerical simulations, and it is expected to be a generic feature of excitation propagation in linear arrays of mutually coupled excitators. Only synchronized excitation patterns, *i.e.* patterns characterized with $\sigma_2 = \sigma_3$, were detected in experiments, and only a few small regions of occurrence of the unsynchronized patterns with $\sigma_3 < \sigma_2$ were encountered in numerical simulations. These results indicate that the linear three-array of the coupled BZ excitators mimics for the most part excitatory patterns in two coupled cells.[35] The value of the threshold of excitability exhibits strong effects on richness of the observed excitatory patterns: only a few fundamental regimes (with firing vectors (1,1,1), (1,0,0), and (0,0,0)) are encountered at suppressed excitability, *i.e.* at high value of the threshold of excitability. The number of the observed patterns increase explosively at low values of the threshold of excitability.

The agreement between experimentally determined and numerically simulated excitation diagrams is satisfactory; only a few unsynchronized partial propagation regimes encountered in numerical simulations were not detected in the experiments. The complex hierarchical structure of occurrence of excitation regimes within the parametric space enables the coupled (reaction) cells to control in a subtle way their mutual communication via proper tuning of the control parameters. Preliminary calculations of propagation patterns in larger cell arrays (more than three units) with various kinetic models exhibit similar behavior as observed in the three-array with the BZ reaction.

Acknowledgment. The authors thank the Grant Agency of the Czech Republic (Grant No. 203/96/1507) and the Ministry of Education of the Czech Republic (Grant No. VS96073) for financial support of this project. The authors are grateful to Dr. I. Schreiber for valuable discussions and suggestions concerning this paper.

References and Notes

(1) Collins, J. J.; Stewart, I. *Biol. Cybern.* **1993**, *68*, 287.
(2) Collins, J. J.; Stewart, I. *Biol. Cybern.* **1994**, *71*, 95.
(3) Batchelor, A. M.; Garthwaite, J. *Nature* **1997**, *385*, 207.
(4) Koch, C. *Nature* **1997**, *385*, 207.
(5) Yoshikawa, K.; Fukunaga, K.; Kawakami, H. *Chem. Phys. Lett.* **1990**, *174*, 273.
(6) Laplante, J.-P.; Pemberton, M.; Hjelmfelt, A.; Ross, J. *J. Phys. Chem.* **1995** *99*, 10063.
(7) Marek, M.; Stuchl, I. *Biophys. Chem.* **1975**, *3*, 241.
(8) Nakajima, K.; Sawada, Y. J. *J. Chem. Phys.* **1980**, *72*, 2231.
(9) Bar-Eli, K.; Reuveni, S. J. *J. Phys. Chem.* **1985**, *89*, 1329.
(10) Bar-Eli, K. *J. Phys. Chem.* **1984**, *88*, 3616.
(11) Boukalouch, M.; Elezgaray, J.; Arneodo, A.; Boissonade, J.; De Kepper; P. *J. Phys. Chem.* **1987**, *91*, 5843.
(12) Crowley, M. F.; Epstein, I. R. *J. Phys. Chem.* **1989**, *93*, 2496.
(13) Stuchl, I.; Marek, M. *J. Chem. Phys.* **1982**, *77*, 1607.
(14) Laplante, J.-P.; Erneux, T. *J. Phys. Chem.* **1992**, *98*, 6537.
(15) Booth, V.; Erneux, T.; Laplante, J.-P. *J. Phys. Chem.* **1994**, *98*, 6537.
(16) Doumbouya, S. I.; Schneider, F. W. *J. Phys. Chem.* **1993**, *97*, 6945.
(17) Doumbouya, S. I.; Münster, A. F.; Doona, C. J.; Schneider, F. W. *J. Phys. Chem.* **1993**, *97*, 1025.
(18) Hauser, M. J. B.; Schneider, F. W. *J. Chem. Phys.* **1994**, *100*, 1058.
(19) Zeyer, K.-P.; Holz, R.; Schneider, F. W. *Ber. Bunsen-Ges. Phys. Chem.* **1993**, *97*, 1112.
(20) Yoshimoto, M.; Yoshikawa, K.; Mori, Y. *Phys. Rev.* E **1993**, *47*, 864.
(21) Weiner, J.; Schneider, F. W.; Bar-Eli, K. *J. Phys. Chem.* **1989**, *93*, 2704.
(22) Chevalier, T.; Freund, A.; Ross, J. *J. Chem. Phys.* **1991**, *95*, 308.
(23) Roesky, P. W.; Doumbouya, S. I.; Schneider F. W. *J. Phys. Chem.* **1993**, *97*, 398.
(24) Weiner, J.; Holz, R.; Schneider, F. W.; Bar-Eli, K. *J. Phys. Chem.* **1992**, *96*, 8915.
(25) Holz, R.; Schneider, F. W. *J. Phys. Chem.* **1993**, *97*, 12239.
(26) Crowley, M. F.; Field, R. J. *J. Phys. Chem.* **1986**, *90*, 1907.
(27) Botré, C.; Lucarini, C.; Memoli, A.; D'Ascenzo, E. *Bioelectrochem. Bioenerg.* **1981**, *8*, 201.
(28) Schneider, F. W.; Hauser, M. J. B.; Reising, J. *Ber. Bunsen-Ges. Phys. Chem.* **1993**, *97*, 55.
(29) Zeyer, K.-P.; Münster, A. F.; Hauser, M. J. B.; Schneider, F. W. *J. Chem. Phys.* **1994**, *101*, 5126.
(30) Marek, M.; Schreiber I. Chaos in Forced and Coupled Oscillators and Excitators, In *Chaos in Chemistry and Biochemistry*; Field, R. J.; Györgyi, L., Eds.; World Scientific: Singapore, 1993; p 87.
(31) Dolník, M.; Finkeová, J.; Schreiber, I.; Marek, M. *J. Phys. Chem.* **1989**, *93*, 2764.
(32) Finkeová, J.; Dolník, M.; Hrudka, B.; Marek, M. *J. Phys. Chem.* **1990**, *94*, 4100.
(33) Dolník, M.; Marek, M. *J. Phys. Chem.* **1991**, *95*, 7262.
(34) Dolník, M.; Marek, M.; Epstein, I. R. *J. Phys. Chem.* **1992**, *96*, 3218.
(35) Kosek, J.; Marek, M. *J. Phys. Chem.* **1993**, *97*, 120.
(36) Kosek, J.; Schreiber, I.; Marek, M. *Phil. Trans. R. Soc. London* A **1994**, *347*, 643.
(37) Dolník, M.; Kosek, J.; Votrubová, V.; Marek, M. *J. Phys. Chem.* **1994**, *98*, 3707.
(38) Alexander, J. C.; Doedel, E. J.; Othmer, H. G. *SIAM J. Appl. Math.* **1989**, *50*, 1373.
(39) *The Dynamics of Excitable Media*; Othmer, H. G., Ed.; Amer. Math. Soc.: Providence, 1990.
(40) *Nonlinear Wave Processes in Excitable Media*; Holden, A. V., Markus, M., Othmer, H. G., Eds.; Plenum Press: New York, 1991.
(41) Zhabotinsky, A. M.; Buchholtz, F.; Kiyatkin, A. B.; Epstein, I. R. *J. Phys. Chem.* **1993**, *97*, 7578.
(42) Robertson, E. B.; Dunford, H. B. *J. Am. Chem. Soc.* **1964**, *86*, 5080.
(43) Kosek, J.; Schreiber, I.; Marek, M. *Phil. Trans. R. Soc. London A* **1995**, *347*, 643.
(44) Somers, D.; Koppel, N. *Physica* **1995**, *D89*, 169.
(45) Dutt, A. K.; Menzinger, M. *J. Phys. Chem.* **1992**, *96*, 8447.
(46) Ruoff, P. *J. Phys. Chem.* **1993**, *97*, 6405.
(47) Gardiner, C. W. *Stochastic Methods for Physics, Chemistry and Natural Sciences*; Springer: Berlin, 1985.
(48) Kloeden, P. E.; Platen, E. *Numerical Solution of Stochastic Differential Equations*; Springer: Berlin, 1995.
(49) Hasal, P.; Kudrna, V. *Collect. Czech. Chem. Commun.* **1996**, *61*, 512.
(50) Marek, M.; Schreiber, I. *Chaotic Behavior of Deterministic Dissipative Systems*; Cambridge Univ. Press: Cambridge, 1995.